AJEHE
Avicenna Journal of Environmental Health Engineering
Avicenna J Environ Health Eng. 2025;12(2):x-x. doi:10.34172/ajehe.5614
http://ajehe.umsha.ac.ir

Original Article

# Efficient Nitrate Removal from Water Using Zinc-Aluminium Layered Double Hydroxide Nanostructures: Synthesis and Adsorption Optimization

**Malika Safi[1*], Mohamed Bouchekara[1], Mohamed Sassi[2], Ahmed Halfadji[3]**

[1]Process Engineering and Solution Chemistry Laboratory (LGPCS), University of Mustapha Stambouli, Mascara, Algeria
[2]Laboratory of Chemistry of Materials (LCM), University of Ahmed BenBella, Oran, Algeria
[3]Department of Science and Technology, Faculty of Applied Sciences, Ibn-khaldoun University of Tiaret, Tiaret, Algeria

**Article history:**
**Received:** February 4, 2025
**Revised:** March 30, 2025
**Accepted:** August 21, 2025
**ePublished:** xx x, 2025

***Corresponding author:**
Malika Safi,
Email: medfadji2021@aol.com

**Abstract**
Layered double hydroxides (LDHs), distinguished by their lamellar nanosheet structures, are highly effective materials for hosting and intercalating functional chemicals, making them suitable for water contaminant remediation. Elevated nitrate ($NO^{3-}$) levels in water and wastewater, attributed to the high solubility of nitrates, pose significant risks to aquatic ecosystems and human health. This study outlined a simple co-precipitation method for synthesizing zinc-aluminum Zn-Al-LDHs and evaluated their performance in efficiently removing nitrate ions under optimal conditions. The characterization of the Zn-Al-LDH nanostructures was conducted through various techniques, including X-ray diffraction (XRD), thermogravimetric and differential thermal analyses (TGA/DTA), scanning electron microscopy (SEM), and Fourier-transform infrared spectroscopy (FTIR). Key parameters influencing nitrate adsorption, such as $NO^{3-}$ concentration, pH, adsorbent dosage, contact time, and temperature, were thoroughly examined in a systematic manner. Notably, the calcined form of LDH (Zn-Al-LDH-C) exhibited the highest nitrate adsorption capacity of 94%, with optimal adsorption at pH 6.9 and low temperature. Equilibrium was reached in 80 minutes, and the adsorption capacity rose to 16 mg/g. FTIR analysis confirmed the intercalation of nitrate ions into the calcined material. Adsorption isotherm studies revealed that nitrate adsorption onto Zn-Al-LDH followed the Langmuir model ($R^2=0.99$), indicating a uniform surface and monolayer adsorption mechanism, as opposed to the Freundlich model ($R^2=0.90$). This study demonstrates the potential of enhancing Zn-Al-LDH-C nanostructures to improve their efficiency in removing contaminants from water and wastewater, presenting a promising approach for advanced water treatment solutions.
**Keywords:** Nitrate removal, Water, Zn-Al-LDH nanostructures, Adsorption optimization, LDH, Calcination effect, Langmuir, and Freundlich

**Please cite this article as follows:** Safi M, Bouchekara M, Sassi M, Halfadji A. Efficient nitrate removal from water using zinc-aluminium layered double hydroxide nanostructures: synthesis and adsorption optimization. Avicenna J Environ Health Eng. 2025;12(2):x-x. doi:10.34172/ajehe.5614

## 1. Introduction

Environmental pollution due to urbanization, industrialization, and intensive agriculture has degraded ecosystems and threatens human health, with contaminants like pesticides, PCBs, PAHs, nitrates, metals, and metalloids increasingly affecting water quality (1,2). Water and wastewater pollution involves diverse chemicals from human activities, contaminating sources, rivers, and supplies (3,4). Nitrate is an important contaminant of groundwater and surface water resources due to its solubility and varied sources. While vital for growth, excess nitrate impairs oxygen transport and remains a key target for removal from soil and water (5,6). Exposure to nitrate can cause serious health problems, including methemoglobinemia (blue baby syndrome) and birth defects (7). These risks have prompted regulations targeting sources such as agriculture, fertilizers, and organic waste (8). Nitrate pollution arises from point and nonpoint sources, mainly agricultural runoff from livestock waste and fertilizers. Factors such as topography, herd density, and buffer zones affect accumulation. Intensive farming increases runoff, causing eutrophication and degrading drinking water quality (9). Nitrate exposure above 10 mg/L poses serious risks to infants,

including methemoglobinemia and developmental issues. Chronic exposure is linked to thyroid disorders, cancer, and birth defects, highlighting the importance of regular water monitoring (10). Nitrate in drinking water raises health concerns, as dietary nitrates are converted into nitrites by oral bacteria, which impair blood function and form carcinogenic nitrosamines, recognized since 1956 (11). Methods like ion exchange and reverse osmosis are used for the removal of nitrate, and ion-exchange resins are most effective. Efficiency depends on competing ions, with new techniques improving results (12).

Adsorption is a cost-effective method for the removal of nitrate, utilizing high surface area, porous adsorbents with ion-exchange sites. Modifications enhance active sites, selectivity, and capacity, allowing rapid pollutant removal with minimal post-treatment (13,14). The adsorption process, in particular, has proven to be one of the most effective techniques for removing several anions, such as fluoride (15), phosphate (16), ammonia (16), nitrate (16), aniline (17), and perchlorate (18), using different adsorbents. The selection of a suitable material plays a vital role in the optimal adsorption of particular pollutants (19).

The high cost of activated carbon has shifted interest to affordable LDHs, valued for their tunable properties and broad applications. Foundational studies were conducted by Feitknecht (1942) and Reichle (1968) (20,21). LDHs, or anionic clays, have the general formula $(M^{II}_{(1\_y)} M^{III}_{y}(OH)_2)^{y+}_{(y/m)}A^{m}\text{-}\ xH_2O$. Their positively charged layers, formed by substituting divalent with trivalent metal ions, provide high ion-exchange capacity for inorganic and organic anions. Typically, $M^{2+}$represents divalent cations like $Mg^{2+}$, $Zn^{2+}$, or $Cu^{2}$ (22), and $M^{3+}$refers to a trivalent cation, which includes ions, such as $Al^{3+}$, $Cr^{3+}$, $Fe^{3+}$(23), and so on. Moreover, the partial substitution of $M^{3+}$for $M^{2+}$results in positively charged hydroxide sheets that require intercalation with anions ($A^{n-}$), such as $CO_3^{2-}$, $NO_3^{-}$, and $Cl^{-}$. LDH nanostructures exhibit characteristics advantageous for pollutant adsorption, including large surface areas, good thermal stability, and elevated sorption and regeneration efficiencies (24). LDHs are cost-effective to synthesize and efficiently treat dye and industrial wastewater. The removal of nitrate depends on optimizing contact time, dose, concentration, pH, and temperature (25).

Recent studies show that biomaterials such as chitosan-modified Mg-Al LDH can remove up to 98.7% of nitrate in 90 minutes at 298 K (26). Calcined Ti nanopores used as electrodes removed 87.5% of nitrate via electrolysis (27). Co-biochar functionalized with Mg/Al LDH nanocomposites showed 86%–100% efficiency and superior durability compared to guava seed/beetroot peel biochar (28). Other effective materials for enhancing nitrate and nitrite adsorption include nano γ-alumina, magnetite-alumina nanocomposites, nZVI/LDH composites, and protonated crosslinked chitosan adsorbents (29,30).

The present study included the following steps. First, zinc-aluminum layered double hydroxides (Zn-Al-LDHs) were effectively produced using a co-precipitation technique. Then, Zn-Al-LDH nanostructure was characterized using various techniques, including X-ray diffraction (XRD) and Fourier-transform infrared spectroscopy (FTIR). Afterwards, to enhance the nitrate adsorption efficiency of the Zn-Al-LDH nanostructure, it is essential to examine the influence of several factors, including pH, contact duration, adsorbent dosage, and nitrate concentration. The effects of the calcination process on Zn-Al-LDH and the influence of temperature (10 to 50 °C) on nitrate adsorption were then investigated. Finally, the equilibrium adsorption data were evaluated through the application of Langmuir and Freundlich isotherm models.

## 2. Materials and Methods

### *2.1. Materials*

The synthesis of LDHs included the use of zinc chloride ($ZnCl_2$), aluminum chloride ($AlCl_3$), sodium hydroxide (NaOH), and sodium carbonate ($Na_2CO_3$). Zinc chloride and aluminum chloride were obtained from Sigma-Aldrich, whereas sodium hydroxide and sodium carbonate were obtained from Merck and Sigma-Aldrich, respectively.

### *2.2. Synthesis of Zn-Al-CO3 Layered Double Hydroxides (Zn-Al-LDH)*

The Zn-Al-LDH, specifically [Zn-Al-$CO_3$], was synthesized through a straightforward co-precipitation technique maintained at a stable pH of 10. In summary, a metal salt solution was prepared by combining precise quantities of salt, which include 20.86 g of $ZnCl_2$, and 12.19 g of $AlCl_3$ dissolved in 50 mL of distilled water (31,32). The precipitation was then induced by dropwise addition of an aqueous solution containing 6 g of NaOH and 10.7 g of $Na_2CO_3$ in 50 mL of distilled water. The pH was maintained at 10 under vigorous stirring until a gel formed. After 18 hours of curing at 70 °C, the synthetic product underwent multiple filtration and washing processes using distilled water and ethanol. Subsequently, the product was dried at 60 °C for 24 hours. After finely grinding with an agate mortar, the obtained sample was calcined at 400 °C (31,32). The synthesized Zn-Al-LDH samples were characterized by XRD and FTIR spectroscopy before use.

### *2.3. Characterizations of the Adsorbent*

The crystallized structures of Zn-Al-LDH before and after nitrate adsorption, as well as those of the zinc-based materials, were characterized by XRD spectroscopy (PANalytical X-Ray Diffractometer). A copper anticathode emitting X-rays with a wavelength of 1.5418 Å was used. FTIR is a technique that relies on the absorption of infrared radiation by the sample under investigation. This method facilitates the identification

of distinctive vibrational modes associated with chemical bonds between atoms, thereby enabling the analysis of various chemical functionalities. The Zn-Al-LDH samples at different stages (before and after nitrate adsorption) were analyzed by a Perkin-Elmer Spectrum 65 Fourier Transform Spectrophotometer. The spectral range was 4000 cm $^{-1}$ to 400 cm $^{-1}$ after pelletization (KBr) with a resolution of 4 cm$^{-1}$. The thermogram was obtained using a SENSYevo SETARAM instrument. For these analyses, the temperature was systematically elevated from 10 °C to 1000 °C at a regulated heating rate of 10 °C/min.

### *2.4. Adsorption Experiments*

A stock solution of nitrates ($NO_3^-$) with 1000 mg/L was prepared using potassium nitrate ($KNO_3$). Then, different proportions were diluted in distilled water to make standard solutions for the determination of nitrates, as well as for the preparation of lower concentration solutions used during the adsorption tests. Additionally, the spectrophotometer was used to measure optical density directly. Moreover, the analyses were carried out on a spectrophotometer UV-vis Spectrum instruments (SP-UV 2005). The highest recorded wavelength for nitrate is λmax = 220 nm. Stock solutions with a concentration of 1 g/L of $NO_3^-$ were prepared by dissolving the required quantity of nitrate in distilled water. Generally, the concentrations achieved through dilution were used in this study. The adsorption experiments were conducted using a series of 250 mL beakers, each containing 20 mg of the respective Zn-Al-LDH and 250 mL of the nitrate solution at the specified concentration. The experiments were conducted at a constant agitation speed of 500 rpm. The pH of the solution was systematically varied between 2 and 12, while the contact time was adjusted from 5 to 360 minutes, and the initial nitrate concentration ranged from 20 to 1000 mg/L. The pH was adjusted to the desired level through the addition of either 1 N HCl or 1 N NaOH. Following each adsorption trial, the solid phase was isolated from the liquid phase via centrifugation at 3000 rpm for 15 minutes. The residual concentrations were assessed using UV-visible spectroscopy. The quantities adsorbed at equilibrium (qe) and at any given time ($q_t$) were computed using the specified following equation (33):

$$q_e = \frac{(C_0 - C_e).V}{m} \quad (1)$$

$q_e$ = Adsorbate concentration at equilibrium, mg/g
$C_o$ = Initial adsorbate concentration, mg/L
$C_e$ = Final adsorbate concentration at equilibrium, mg/L
V = Volume of liquid, L
m = Mass of Zn-Al-LDH adsorbent, g

## 3. Results and Discussion

### *3.1. Characterizations of the Sorbent*

Fig. 1a illustrates the XRD pattern of synthesized Zn-Al-LDH, which is typical of hydrotalcite-like compounds,

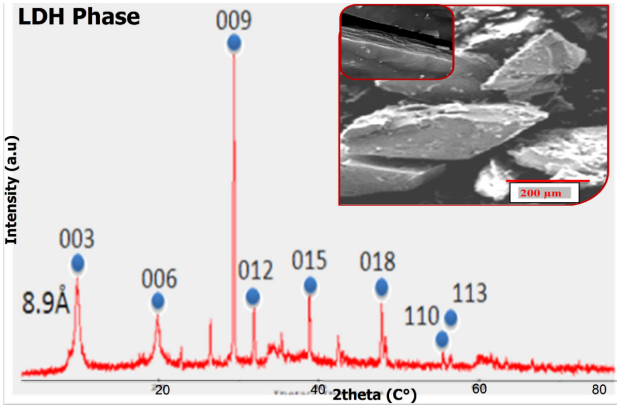


**Fig. 1**. (**a**) X-ray Diffraction Patterns and (**b**) **(inset)** SEM Analysis of the Synthesized Zinc-Aluminum Layered Double Hydroxide (Zn-Al-LDH)

with diffraction peaks at 2θ: 31.2°, 34.1°, 39.4°, and 53.6° attributed to the (009), (012), (015), and (018) planes, respectively, which are characteristics of the LDH structure. Additionally, the XRD pattern further reveals prominent symmetric reflection planes corresponding to (00l) and (11l), which suggest the distribution of metal ions within the LDH. Additionally, a less intense and asymmetric (01l) plane was observed, which can be classified within a hexagonal lattice structure characterized by rhombohedral space group symmetry, denoted as R $\bar{3}$ m rhombohedral. The intense reflection peaks observed at low 2θ angles (10.45°–21.89°) were affected by the dimensions of the intercalated anion ($CO_3^-$) and yielded insights into the basal spacing, facilitating the calculation of the lattice parameter (c). Additionally, the prominent reflection at (110) corresponding to 2θ (57.67°) provided information regarding the average cation-cation distance, thereby enabling the determination of the lattice parameter (a) (34). The lattice parameters a and c are detailed in Table 1. Additionally, the observed profiles were modeled as two-phase mixtures consisting of wurtzite ZnO and spinel $ZnAl_2O$. These results confirm that the prepared material is the Zn-Al-LDH and are entirely consistent with the literature (35,36).

The previous SEM analysis of the Zn-Al-LDH nanostructure (Fig. 1b) indicated that the particles were extensively interconnected and displayed a distinct layered architecture, with the plate-like particles uniformly dispersed. The surface appeared to be flat with a layered texture, which makes the pockets rough and porous. This indicates that the material has excellent properties for use as an effective adsorbent of nitrate ions (37).

The FTIR spectrum obtained for the Zn-Al-layered double hydroxide (ZnAl-$CO_3$), as illustrated in Fig. 3 , displays bands that are indicative of hydrotalcite-like materials (34). We can illustrate the broad and strong band centered at 3400 cm$^{-1}$, which is associated with the stretching vibrations of the OH bonds present in hydroxyl groups and water molecules ($H_2O$). Additionally, the weaker band at 1630 cm$^{-1}$ is attributed to the bending vibrations of $H_2O$ within the interlayer spaces. This can also be attributed to C = C from the conjugated (aromatic)

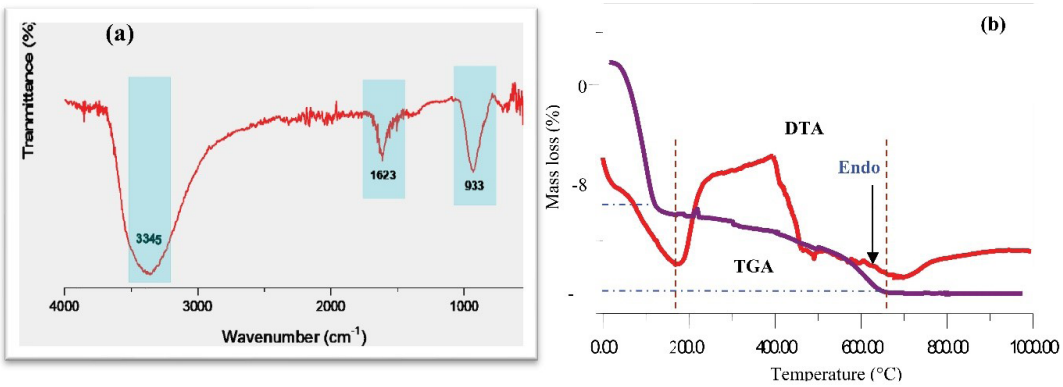


**Fig. 2.** a) IR Spectrum of Zn-Al-LDH, b) DTG/DTA Analysis of Zn-Al-LDH

**Table 1.** Crystallographic Data of Synthesized Zn-Al-LDH

| LDH | $d_{003}$(Å) | $d_{110}$ (Å) | Lattice parameters* | | Average size (nm) |
|---|---|---|---|---|---|
| | | | a | c | |
| ZnAl-LDH | 8.91 | 1.55 | 3.10 | 26.73 | 50 |

* $c = 3/2[d_{003} + 2d_{006}]$ and $a = 2d_{110}$

alkene group (37). The spectral bands observed at 460, 550, and 790 $cm^{-1}$ are associated with the condensed Al—O groups, the translation of Zn/Al—OH, and the deformation of Al—OH, respectively. In the case of the Zn—Al—$CO_3$ sample, the band observed near 1365 $cm^{-1}$ corresponds to the antisymmetric stretching mode of the carbonate ion, while the bands detected around 870 and 680 $cm^{-1}$ are linked to the weak non-planar bending mode and the angular bending mode of carbonate, respectively. According to Fig. 2a, the spectrum of the LDH phases has three characteristic domains, 4000-2500 $cm^{-1}$, and visible bands, located around 3400-3600 $cm^{-1}$. The vibrations associated with the hydroxyl groups (υOH) of the sheet, as well as those of water molecules that are physisorbed and intercalated, are the focus of this discussion. For low frequencies, $\nu < 1000$ $cm^{-1}$, the observed vibration bands were assigned to the network. Additionally, the valence vibrations ($\nu_{M-O}$) between the metal and the oxygen atoms (568 and 617 $cm^{-1}$) were distinguished; therefore, for the LDH phase [Zn—Al—$CO_3$] that we synthesized, the wide band located between 3100 and 3700 $cm^{-1}$ was attributed to valence vibration of OH-groups (OH ... ..OH) of physiosorbed water and/or valence vibration of OH— (M—OH) groups linked to carbonate anions in the presence of divalent cations and trivalent ($Zn^{+2}$ and $Al^{+3}$). The weak band centered at 1623 $cm^{-1}$ corresponded to the deformation vibration mode of water molecules strongly adsorbed between the layers. The carbonate anions were characterized by three frequency bands (i.e., 1415 $cm^{-1}$, 880 $cm^{-1}$, and 680 $cm^{-1}$) in our sample; these bands were shifted towards 1500$cm^{-1}$, which can be attributed to the reorganization of the $CO_3^{2-}$ anions within the interlayer region when water molecules are present (38,39).

### *3.2. DTG/DTA Analysis of Zn-Al-LDH*

The thermal decomposition of Zn-Al-LDH was investigated using thermogravimetric analysis (TGA) and differential thermal analysis (DTA) to better understand its decomposition behavior. The thermogravimetric and differential thermal analysis (DTG/DTA) results, as illustrated in Figure 2b, demonstrate that the decomposition of Zn-Al-LDH proceeds through two clearly defined endothermic stages. The preliminary phase, which occurs at approximately 250°C, is attributed to the evaporation of water adsorbed on the surface as well as the removal of intercalated water molecules from the material. The next phase, occurring at 450°C, is characterized by the dehydroxylation of the structural layers, which leads to the disintegration of the lamellar structure and the formation of a mixed metal oxide (40). A minor thermal peak was observed at higher temperatures near 650 °C, which was attributed to the elimination of residual carbonate ions strongly bound to the brucite layers (40). The dehydroxylation process,

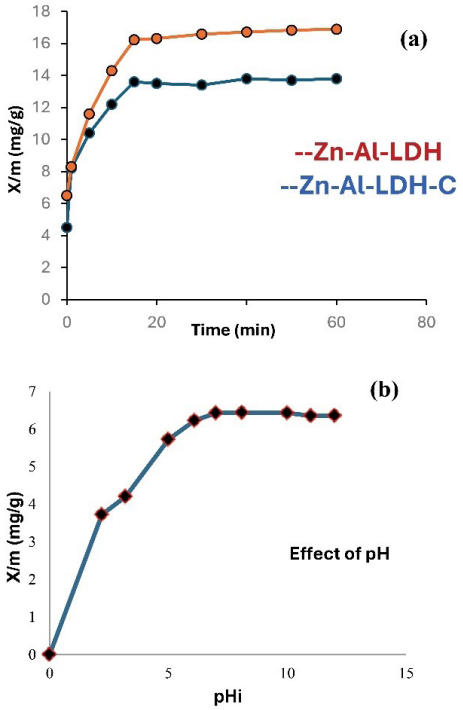


**Fig. 3.** (a) Effects of Contact Time and (b) pH on the Surface Adsorption of Nitrate on Zn-Al-LDH and Zn-Al-LDH-C

along with the decomposition of interlayer carbonate ions ($CO_3^{2-}$), contributed to a mass loss of 32.5% up to 420 °C. Additionally, the structural deformation of the lamellae and the appearance of metal oxides were evident at 650 °C. The DTA curve shows three distinct endothermic peaks, each associated with the decomposition of interlayer anions.

### 3.3. Adsorption Evaluations of Zn-Al-LDH

#### 3.3.1. The Effect of Contact Time on Nitrate Adsorption by Uncalcined Zn-Al-LDH and Calcinated Zn-Al-LDH-C

Fig. 3a illustrates the experimental findings, indicating that the surface adsorption of nitrate was enhanced on both Zn-Al-LDH and calcined Zn-Al-LDH-C. The adsorption process is characterized by two separate stages: an initial rapid phase followed by a more gradual phase. The amount of nitrate adsorbed increased with contact time. The curve indicates a rapid increase in the rate of nitrate removal within the first 30 minutes, reaching equilibrium after approximately 80 minutes. At equilibrium, the Zn-Al-LDH exhibited a maximum adsorption capacity of 13 mg/g.

In contrast, Zn-Al-LDH-C exhibited an enhanced adsorption capacity, reaching a peak of 16 mg/g within 80–100 minutes in our study. This contrasts with a similar study that used calcined Mg-Al-LDH, which achieved a nitrate removal efficiency of 84% from real water. However, in the second stage, after the elimination of cations with a dose of 20 g/L, the efficiency increased to 99% (41). The enhanced performance of Zn-Al-LDH-C suggests its higher affinity for nitrate, likely due to its interlamellar spacing and the availability of primary adsorption sites, which were effectively occupied during the process.

#### 3.3.2. The Effect of pH on the Adsorption of Nitrate with Zn-Al-LDH

Generally, pH is widely recognized as a significant parameter influencing the adsorption process at the interface between water and the adsorbent. To investigate this effect, adsorption experiments were conducted under consistent experimental conditions while systematically varying the solution pH from 2 to 12. The results of these experiments are presented in Fig. 3b. The representation of the effect of pH allows for the optimization of pH for the maximum adsorbed quantity of nitrate on the Zn-Al-LDH. It can be observed that the adsorbed quantity increased as pH was increased and that it reached the maximum value at pH 6.9. Therefore, the best pH for adsorption was 7. The findings indicate that the adsorption of nitrate anion ($NO_3^-$) on Zn/Al-LDH surfaces decreased with increasing pH beyond this optimum, aligning with previous studies on Zn-Al-LDH synthesized using the co-precipitation method at a Zn/Al molar ratio of 3:1 (42). Furthermore, Li et al reported that pH is the most influential factor in the efficient adsorption of organic contaminants from wastewater using Zn-Al-LDH (43).

#### 3.3.3. The Effect of the Dosage of Adsorbent on the Adsorption of Nitrate with Zn-Al-LDH

The obtained results are shown in Fig. 4. The data for both samples indicate that the adsorption capacity increased with increasing initial concentration. Consequently, the adsorption quantity increased as the concentration of the examined solution was increased.

#### 3.3.4.1. Influence of Temperature on Nitrate Adsorption

Understanding the effect of temperature on the adsorption of ions from a solution is essential for enhancing the efficiency of the adsorption process. The nitrate adsorption isotherms at 10 °C, 25 °C, and 50 °C are illustrated in Fig. 5a. These findings confirm the exothermic characteristics associated with the adsorption of nitrates onto the synthesized Zn-Al-LDH, as evidenced by increased adsorption at lower temperatures.

This behavior is consistent with the surrounding environmental conditions, as significant nitrate leaching generally takes place during colder, wetter, and non-growing periods, especially from late autumn to early spring. The enhanced nitrate adsorption at lower temperatures highlights the significant advantage of using LDH materials for the removal of nitrate, making it an effective solution under such conditions. The results showed that the adsorption of nitrate anions ($NO_3^-$) on the surface of Zn/Al-LDH decreased with rising temperature, similar to findings from a study where Zn-Al-LDH was synthesized using the co-precipitation method at a Zn/Al molar ratio of 3:1 (42). However, Mohammadi et al reported that an increase in temperature leads to a decrease in nitrate adsorption on activated carbon (44). Similarly, the adsorption efficiency of Zn–Mg–Al/LDH has been observed to decrease as the temperature rises (45).

#### 3.3.4.2. Effect of Calcination (FTIR Characterization)

As illustrated in Fig. 5b, the FTIR analysis of Zn-Al-LDH before and after calcination (Zn-Al-LDH and Zn-Al-LDH-C) reveals that the calcination process significantly affects the adsorption characteristics of Zn-Al-LDH. A

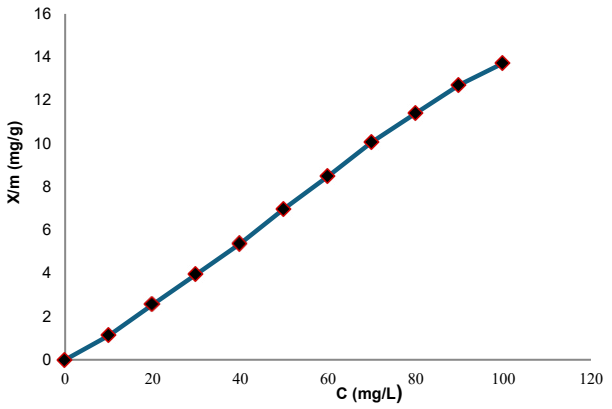


**Fig. 4.** The Impact of Adsorbent Concentration (C) on the Surface Adsorption of Nitrate onto Zn-Al-LDH

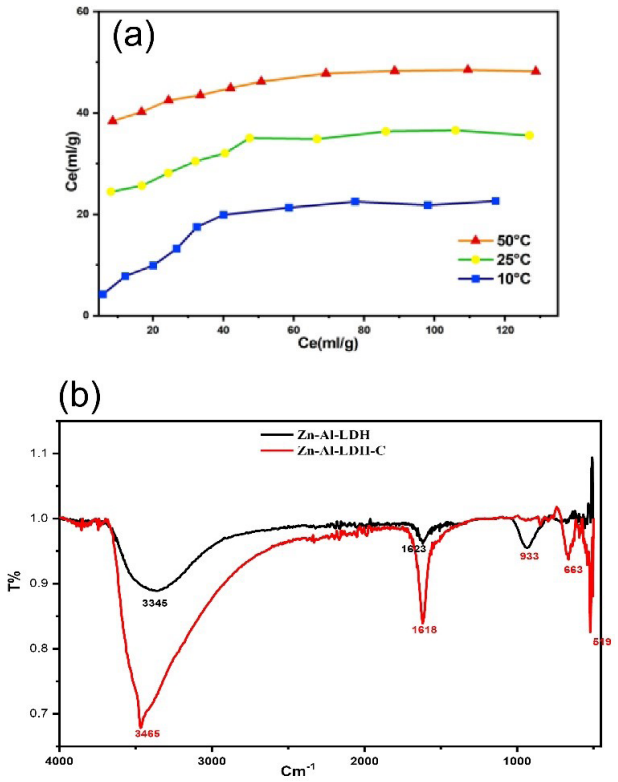


**Fig. 5.** (a) Influence of Temperature on Adsorption of Nitrate, (b) FTIR Spectra of Uncalcined Material (Zn-Al-LDH) and Calcinated Material (Zn-Al-LDH-C)

significant reduction in the intensity of all adsorption peaks is observed following calcination. Notably, the band corresponding to interlayer water molecules ($\nu_{H2O}$) at approximately 1618 $cm^{-1}$ exhibits a decrease in intensity, indicating their removal. Furthermore, the vibration band associated with carbonate anions ($\nu_3(CO_3)$) becomes broader and exhibits a lower intensity compared to the uncalcined LDH phase, reflecting the expulsion of carbonate ions, typically in the form of $CO_2$, during the dehydration of the Zn-Al-LDH structure. Upon rehydration, the interlamellar space accommodates reintroduced water molecules and carbonate anions ($CO_3^{2-}$), leading to the reconstruction of a new LDH phase. This demonstrates the reversible nature of the structural changes and the ability of the material to restore its intercalated components.

Table 2 compares LDH-based materials for nitrate removal from water, focusing on synthesis conditions, pH, dose, efficiency, and cost. Calcined materials such as Zn-Al-LDH-C and Mg-Al-LDH-C (400-500 °C) showed enhanced stability, while non-calcined ones (Zn-Al-LDH@BBAC, Mg-Al-LDH@Biochar) may have altered surface properties.

Nitrate removal was most effective at pH 6-7, with Zn-Al-LDH-C achieving the highest efficiency (94%) at a low dose, whereas Mg-Al-LDH@Biochar had the lowest (70%) despite a longer reaction time. Most LDH-based materials were low-cost, except for biochar composites, which had moderate costs. Zn-Al-LDH-C proved the most efficient and cost-effective option.

### *3.3.5. Adsorption Isotherm*

The adsorption isotherms were obtained using the optimum suspensions of each material studied in 20 mL of nitrate at an initial concentration ranging from 25 to 500 mg/L and at the pH of the solution. The suspensions were stirred for the optimal duration at room temperature, centrifuged, and diluted. Then, the supernatants were analyzed. The adsorption equations of Langmuir and Freundlich were used to investigate the capacity of Zn-Al-LDH in terms of the adsorption of nitrate. The Langmuir model is one of the most important models of one-layer adsorption models, which is based on a constant number of adsorption places, and every place has the ability to receive one molecule of adsorbent. The conditions remained consistent across all locations, and no interactions occurred between the molecules of the adsorbent. Another model for isotherm adsorption is the Freundlich model. These two models are presented as follows (50).

Langmuir: $$q_e = \frac{Q_{max} b C_e}{1 + b C_e} \quad (2)$$

Linear form: $$q_e = Q_{max} - \frac{q_e}{b C_e} \quad (3)$$

Freundlich: $$q_e = K C_e^{1/n} \quad (4)$$

Linear form: $$\log q_e = \log K_f + \frac{1}{n} \log C_e \quad (5)$$

Where $q_e$ represents the quantity of adsorbate (in mg), $C_e$ denotes the equilibrium concentration of the adsorbate in the solution (in mg), $Q_{max}$ indicates the maximum adsorption capacity (in mg/g), and b, k, and n are constants. The surface adsorption of nitrate onto Zn-Al-LDH increased with rising external nitrate concentration. After applying the adsorption models, the constants for each model were computed, and the plots of these data are given in Fig. 6a (Freundlich model) and Fig. 6b (Langmuir model) indicate that the Langmuir equation provides a superior fit for the adsorption isotherms of nitrate onto the Zn-Al-LDH samples, as evidenced by a higher correlation coefficient ($R^2 = 0.994$) compared to the Freundlich isotherm model ($R^2 = 0.909$). These results suggest homogeneous surface characteristics and support the notion of a monolayer formation of nitrate molecules on the adsorbent surfaces. In summary, the $R^2$ correlation coefficients for Langmuir isotherms were found to be greater than those derived from Freundlich isotherms, suggesting that adsorption of nitrate onto Zn-Al-LDH occurs through a monolayer adsorption mechanism.

The infrared spectrum presented in Fig. 7a shows all the characteristic bands of the Zn-Al-LDH phases after the adsorption of the nitrate ions, as clearly demonstrated by the net decrease in the carbonate ion band. It has been reported that the characteristic peak of $NO_3^-$ exists at approximately 1365 $cm^{-1}$. Fig. 7b illustrates the isotherm associated with the adsorption of nitrate onto Zn-Al-LDH.

**Table 2**. Comparison of Nitrate Removal Efficiency and Cost of Various LDH-Based Synthesized Materials

| Synthesized materials based on LDH | Calcination step | pH | Temperature (°) | Time (min) | Dose | Nitrate removal efficiency (%) | Cost | References |
|---|---|---|---|---|---|---|---|---|
| Zn-Al-LDH-C | Yes (at 400°C) | 6.9 | 25 | 80 | 16 mg/g | 94 | Low | This study |
| Mg-Al-LDH-C | Yes (at 500°C) | 6.0 | --- | 180 | 5-20 g/L | 86 | Low | (46) |
| Zn-Al-LDH@BBAC | No (at 70°C) | 7 | --- | 120 | 100 mg/L | 90 | Moderate | (47) |
| Mg-Al-LDH@Biochar | No | 6 | 45 | 840 | 100mg | 70 | Moderate | (48) |
| Zn–Al–Cl LDH | Yes (at 400°C) | 6 | 20 | 45 | 300mg | 85.5 | Moderate | (49) |
| Zn-Al-LDH (4:1) | No (at 180°C) | 7 | --- | 60 | 2 g/L | 78 | Moderate | (44) |

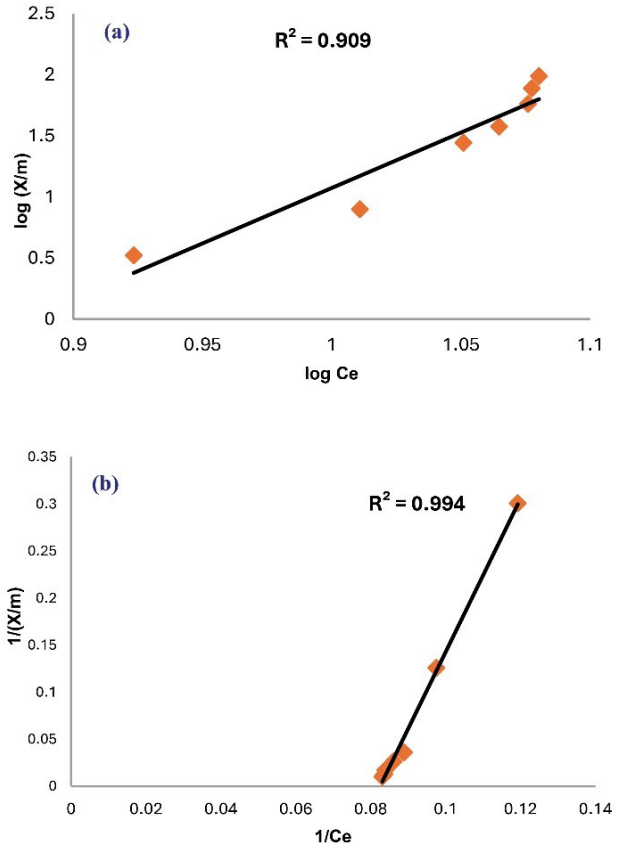


**Fig. 6.** (a) Freundlich Isotherm and (b) Langmuir Isotherm Models

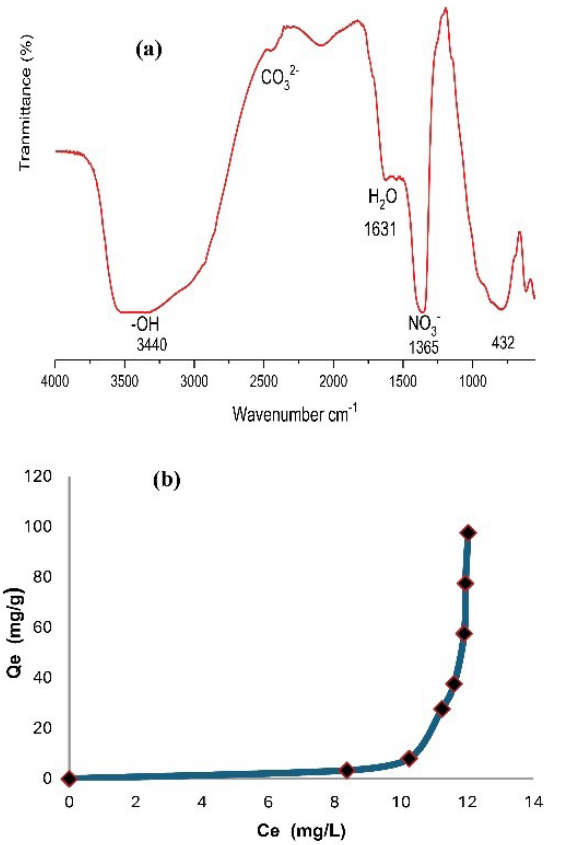


**Fig. 7.** (a) FTIR Spectra of Zn-Al-LDH after Nitrate Adsorption, (b) Isotherm of Nitrate Adsorption on LDH

### *3.3.6. Adsorption Mechanism*

The distinctive properties of Zn-Al-LDHs, including their layered structures, high surface areas, and high ion-exchange capacities, make them highly favored as nanomaterials for the adsorption process. The adsorption processes facilitated by LDHs can occur through various mechanisms, such as surface adsorption, ion exchange, intercalation, and memory reconstruction. When polycationic ions are adsorbed by LDHs, numerous pathways emerge, complicating the task of fully elucidating the different modes or mechanisms through which anions are incorporated. The operational conditions established for the effective removal of nitrate ions included a short contact time, low concentration, and reduced adsorption temperature. The adsorption of $NO_3^-$ onto the (ZnAl-$CO_3$) Zn-Al-LDH is facilitated by p-complexation. This interaction occurs between the zinc ions, which possess available positive charges, and the partially negatively charged oxygen atoms of the $NO_3^-$ ions. Bonding can occur either through direct sigma bonds or via the back donation of electron density from zinc to the nonbonding orbitals of oxygen atoms. The proposed mechanism is consistent with the FTIR analysis of Zn-Al-LDH following the adsorption process. This analysis revealed a significant electrostatic interaction between the layered Zn-Al-LDH and adsorbed nitrate anions. Furthermore, the structural integrity of the Zn-Al-LDH was maintained, as evidenced by the absence of any noticeable changes after nitrate adsorption, indicating both the sustainability and stability of the material. The carbonate group is the most prevalent and stable interlayer anion, accompanied by the consistent presence of certain interlayer water molecules.

The nitrate removal mechanism of Zn-Al-LDH-C includes ion exchange, electrostatic attraction, and intercalation. Calcination enhances adsorption by increasing surface

area and creating structural vacancies. Positively charged hydroxyl groups attract nitrate ions, which intercalate into the LDH layers. FTIR analysis confirms nitrate incorporation, and Langmuir isotherm fitting indicates a uniform monolayer adsorption process.

## 4. Conclusion

This study primarily focused on the synthesis, characterization, and application of Zn-Al-LDH nanostructure derived from a LDH matrix for the removal of nitrate from aqueous environments. The synthesized adsorbent was characterized using XRD, TGA/DTA, SEM, and FTIR to confirm the successful formation of the LDH nanostructure. Before conducting the elimination experiments, we confirmed that the synthesized materials were indeed the desired double-lamellar hydroxides. During the nitrate removal experiments, several parameters influencing the nitrate-removal capacity were examined, including the adsorption kinetics, isotherms, and the effect of solution pH. The elevated $R^2$ value suggested that the data aligned more closely with the Langmuir adsorption model than with the Freundlich model. Zn-Al-$CO_3$-LDHs exhibited significant adsorption capacity for the removal of nitrate from water. The adsorption process showed high nitrate removal efficiency, and the impact of temperature on the adsorption process was found to be significant. Zn-Al-LDH, derived from the original LDH, shows promising potential as an adsorbent catalyst for water treatment. These findings are of practical relevance for optimizing remediation technologies for aquatic environments.

### Authors' Contribution

**Conceptualization:** Malika Safi.
**Data curation:** Mohamed Bouchekara, Malika Safi.
**Formal Analysis:** Mohamed Bouchekara, Mohamed Sassi.
**Funding acquisition:** Mohamed Bouchekara, Mohamed Sassi.
**Investigation:** Mohamed Bouchekara, Malika Safi.
**Methodology:** Malika Safi.
**Project administration:** Mohamed Bouchekara, Mohamed Sassi.
**Resources:** Ahmed Halfadji, Malika Safi.
**Software:** Ahmed Halfadji.
**Supervision:** Mohamed Bouchekara: Mohamed Sassi.
**Validation:** Malika Safi, Ahmed Halfadji.
**Visualization:** Mohamed Bouchekara: Malika Safi, Ahmed Halfadji.
**Writing – original draft:** Ahmed Halfadji, Malika Safi.
**Writing – review & editing:**Malika Safi, Ahmed Halfadji, Mohamed Bouchekara.

### Competing Interests

None declared.

### Ethical Approval

Not applicable.

### Funding

This study was self-funded by the authors and received no external financial support from any funding organization.

### References

1. Iyiola AO, Ipinmoroti MO, Akingba OO, Ewutanure JS, Setufe SB, Bilikoni J, et al. Organic chemical pollutants within water systems and sustainable management strategies. In: Izah SC, Ogwu MC, Loukas A, Hamidifar H, eds. Water Crises and Sustainable Management in the Global South. Singapore: Springer; 2024. p. 211-51. doi: 10.1007/978-981-97-4966-9_7.
2. Halfadji A, Portet-Koltalo F, Touabet A, Le Derf F, Morin C, Merlet-Machour N. Phytoremediation of PCB: contaminated Algerian soils using native agronomics plants. Environ Geochem Health. 2022;44(1):117-32. doi: 10.1007/s10653-021-01049-z.
3. Halfadji A, Naous M, Nadia Kharroubi K, el Zahraà Belmehdi F, Aoudia H. Facile prepared Fe3O4 nanoparticles as a nano-catalyst on photo-Fenton process to remediation of methylene blue dye from water: characterisation and optimization. Glob Nest J. 2023;26(1):05312. doi: 10.30955/gnj.005312.
4. Naous M, Halfadji A. Comparative adsorption study of functionalized magnetite and maghemite nanoparticles coated with CTAB surfactant for efficient chromium removal from wastewater. J Water Environ Nanotechnol. 2024;9(1):73-89. doi: 10.22090/jwent.2024.01.05.
5. Dey S, Haripavan N, Basha SR, Babu GV. Removal of ammonia and nitrates from contaminated water by using solid waste bio-adsorbents. Curr Res Chem Biol. 2021;1:100005. doi: 10.1016/j.crchbi.2021.100005.
6. Moloantoa KM, Khetsha ZP, Van Heerden E, Castillo JC, Cason ED. Nitrate water contamination from industrial activities and complete denitrification as a remediation option. Water. 2022;14(5):799. doi: 10.3390/w14050799.
7. Brender JD. Human health effects of exposure to nitrate, nitrite, and nitrogen dioxide. In: Sutton MA, Mason KE, Bleeker A, Hicks WK, Masso C, Raghuram N, et al, eds. Just Enough Nitrogen: Perspectives on how to get there for regions with too much and too little nitrogen. Cham: Springer International Publishing; 2020. p. 283-94. doi: 10.1007/978-3-030-58065-0_18.
8. Bijay S, Craswell E. Fertilizers and nitrate pollution of surface and ground water: an increasingly pervasive global problem. SN Appl Sci. 2021;3(4):518. doi: 10.1007/s42452-021-04521-8.
9. Luna Juncal MJ, Masino P, Bertone E, Stewart RA. Towards nutrient neutrality: A review of agricultural runoff mitigation strategies and the development of a decision-making framework. Sci Total Environ. 2023;874:162408. doi: 10.1016/j.scitotenv.2023.162408.
10. Lin L, St Clair S, Gamble GD, Crowther CA, Dixon L, Bloomfield FH, et al. Nitrate contamination in drinking water and adverse reproductive and birth outcomes: a systematic review and meta-analysis. Sci Rep. 2023;13(1):563. doi: 10.1038/s41598-022-27345-x.
11. Jain D, Chaudhary P, Varshney N, Janmeda P. Carcinogenic effects of N-nitroso compounds in the environment. Environ Conserv J. 2020;21(3):25-41. doi: 10.36953/ecj.2020.21304.
12. Abascal E, Gómez-Coma L, Ortiz I, Ortiz A. Global diagnosis of nitrate pollution in groundwater and review of removal technologies. Sci Total Environ. 2022;810:152233. doi: 10.1016/j.scitotenv.2021.152233.
13. Pastushok O, Iurchenkova A, Keshavarz F, Barbiellini B, Repo E, Laakso E. Nitrate and phosphate removal by capacitive deionization using nanocellulose/polypyrrole electrodes. Chem Eng Sci. 2025;301:120719. doi: 10.1016/j.ces.2024.120719.
14. Halfadji A, Bennabi L, Giannakis S, Marrani AG, Bellucci S. Sono-synthesis and characterization of next-generation antimicrobial ZnO/TiO2 and Fe3O4/TiO2 bi-nanocomposites, for antibacterial and antifungal applications. Ceram Int. 2024;50(20 Pt B):39097-108. doi: 10.1016/j.ceramint.2024.07.276.
15. Iriel A, Bruneel SP, Schenone N, Cirelli AF. The removal of

fluoride from aqueous solution by a lateritic soil adsorption: Kinetic and equilibrium studies. Ecotoxicol Environ Saf. 2018;149:166-72. doi: 10.1016/j.ecoenv.2017.11.016.
16. Rezaei H, Rastegar S, Naseri S. Application of chitosan and activated carbon nano-composite in removal of nitrite, phosphate, and ammonia from aquaculture wastewater. Avicenna J Environ Health Eng. 2019;6(2):106-12. doi: 10.34172/ajehe.2019.14.
17. Tarlani Azar M, Leili M, Taherkhani F, Bhatnagar A. A comparative study for the removal of aniline from aqueous solutions using modified bentonite and activated carbon. Desalin Water Treat. 2016;57(51):24430-43. doi: 10.1080/19443994.2016.1138890.
18. Bagherifam S, Komarneni S, Lakzian A, Fotovat A, Khorasani R, Huang W, et al. Highly selective removal of nitrate and perchlorate by organoclay. Appl Clay Sci. 2014;95:126-32. doi: 10.1016/j.clay.2014.03.021.
19. Bhatnagar A, Kumar E, Sillanpää M. Nitrate removal from water by nano-alumina: characterization and sorption studies. Chem Eng J. 2010;163(3):317-23. doi: 10.1016/j.cej.2010.08.008.
20. Del Hoyo C. Layered double hydroxides and human health: an overview. Appl Clay Sci. 2007;36(1-3):103-21. doi: 10.1016/j.clay.2006.06.010.
21. de Roy A, Forano C, El Malki K, Besse JP. Anionic clays: trends in pillaring chemistry. In: Occelli ML, Robson HE, eds. Expanded Clays and Other Microporous Solids. Boston, MA: Springer; 1992. p. 108-69. doi: 10.1007/978-1-4615-3534-8_7.
22. Parida KM, Mohapatra L. Carbonate intercalated Zn/Fe layered double hydroxide: a novel photocatalyst for the enhanced photo degradation of azo dyes. Chem Eng J. 2012;179:131-9. doi: 10.1016/j.cej.2011.10.070.
23. Gong M, Li Y, Wang H, Liang Y, Wu JZ, Zhou J, et al. An advanced Ni-Fe layered double hydroxide electrocatalyst for water oxidation. J Am Chem Soc. 2013;135(23):8452-5. doi: 10.1021/ja4027715.
24. Boclair JW, Braterman PS. Layered double hydroxide stability. 1. Relative stabilities of layered double hydroxides and their simple counterparts. Chem Mater. 1999;11(2):298-302. doi: 10.1021/cm980523u.
25. Taoufik N, Elmchaouri A, Korili SA, Gil A. Optimizing the removal of nitrate by adsorption onto activated carbon using response surface methodology based on the central composite design. J Appl Water Eng Res. 2020;8(1):66-77. doi: 10.1080/23249676.2020.1723446.
26. Bansal M, Pal B. Enhanced elimination of nitrate and nitrite ions from ground and surface wastewater using chitosan sphere-modified Mg-Al layered double hydroxide composite. J Ind Eng Chem. 2025;142:635-50. doi: 10.1016/j.jiec.2024.08.007.
27. Meng Y, Tan W, Lv S, Liu F, Xu J, Ma X, et al. Enhanced electrochemical nitrate removal from groundwater by simply calcined Ti nanopores with modified surface characters. Chin J Chem Eng. 2024;75:74-85. doi: 10.1016/j.cjche.2024.07.017.
28. Mahmoud ME, Kamel NK, Amira MF, Fekry NA. Nitrate removal from wastewater by a novel co-biochar from guava seeds/beetroot peels-functionalized-Mg/Al double-layered hydroxide. Sep Purif Technol. 2024;344:127067. doi: 10.1016/j.seppur.2024.127067.
29. Khatamian M, Khadivi Derakhshan S, Hosseini Nami S, Fazli-Shokouhi S. Nitrate removal study of synthesized nano γ-alumina and magnetite-alumina nanocomposite adsorbents prepared by various methods and precursors. Sci Rep. 2024;14(1):7673. doi: 10.1038/s41598-024-58459-z.
30. Pei Y, Cheng W, Liu R, Di H, Jiang Y, Zheng C, et al. Synergistic effect and mechanism of nZVI/LDH composites adsorption coupled reduction of nitrate in micro-polluted water. J Hazard Mater. 2024;464:133023. doi: 10.1016/j.jhazmat.2023.133023.
31. Chang Z, Evans DG, Duan X, Vial C, Ghanbaja J, Prevot V, et al. Synthesis of [Zn–Al–CO3] layered double hydroxides by a coprecipitation method under steady-state conditions. J Solid State Chem. 2005;178(9):2766-77. doi: 10.1016/j.jssc.2005.06.024.
32. Santamaría L, Korili SA, Gil A. Metal-Al layered double hydroxides synthesized from aluminum slags as efficient CO2 adsorbents at pre- and post-combustion temperature. J Environ Chem Eng. 2023;11(5):110936. doi: 10.1016/j.jece.2023.110936.
33. Naous MT, Halfadji AT, Zoubir H. Surfactant chain length's impact on hexavalent chromium adsorption by magnetite nanoparticles. Iran J Chem Chem Eng. 2024;43(4):1550-65. doi: 1021-9986/2024/4/1662-1677.
34. Boubakri S, Djebbi MA, Bouaziz Z, Namour P, Jaffrezic-Renault N, Ben Haj Amara A, et al. Removal of two anionic reactive textile dyes by adsorption into MgAl-layered double hydroxide in aqueous solutions. Environ Sci Pollut Res Int. 2018;25(24):23817-32. doi: 10.1007/s11356-018-2391-6.
35. Sun Y, Zhou Y, Wang Z, Ye X. Structural and morphological transformations of Zn–Al layered double hydroxides through hydrothermal treatment. Appl Surf Sci. 2009;255(12):6372-7. doi: 10.1016/j.apsusc.2009.02.018.
36. Foruzin LJ, Rezvani Z, Nejati K. Fabrication of TiO2@ZnAl-layered double hydroxide-based anode material for dye-sensitized solar cell. RSC Adv. 2016;6(13):10912-8. doi: 10.1039/c5ra23384d.
37. Jamhour RM, Al-Msiedeen AM, Al-Sharaydeh RZ, Jamhour MR, Altweiq AM. Zn-Al layered double hydroxide nanoparticles for efficient removal of food dyes from wastewater. Desalin Water Treat. 2024;317:100036. doi: 10.1016/j.dwt.2024.100036.
38. Arab L, Boutahala M, Djellouli B. Étude de l'élimination du Cr(VI) par l'oxyde mixte obtenu par calcination de l'hydroxyde double lamellaire MgAl. C R Chim. 2014;17(7-8):860-8. doi: 10.1016/j.crci.2014.01.013.
39. Zeng RC, Li XT, Liu ZG, Zhang F, Li SQ, Cui HZ. Corrosion resistance of Zn–Al layered double hydroxide/poly(lactic acid) composite coating on magnesium alloy AZ31. Front Mater Sci. 2015;9(4):355-65. doi: 10.1007/s11706-015-0307-7.
40. Janani FZ, Taoufik N, Khiar H, Elhalil A, Qourzal S, Sadiq M, et al. Effect of Ag doping on photocatalytic activity of ZnO-Al2O3 derived from LDH structure: Synthesis, characterization and experimental study. Appl Surf Sci Adv. 2023;16:100430. doi: 10.1016/j.apsadv.2023.100430.
41. Abbood NS, Ali NS, Khader EH, Majdi HS, Albayati TM, Saady NM. Photocatalytic degradation of cefotaxime pharmaceutical compounds onto a modified nanocatalyst. Res Chem Intermed. 2023;49(1):43-56. doi: 10.1007/s11164-022-04879-3.
42. Salman HE, Hussein NJ. Synthesis of zinc-aluminum layered double hydroxides and application of adsorption for nitrate from water. IOP Conf Ser Mater Sci Eng. 2019;571(1):012070. doi: 10.1088/1757-899X/571/1/012070.
43. Li A, Deng H, Ye C, Jiang Y. Fabrication and characterization of novel ZnAl-layered double hydroxide for the superadsorption of organic contaminants from wastewater. ACS Omega. 2020;5(25):15152-61. doi: 10.1021/acsomega.0c01092.
44. Mohammadi M, Mohammadi Torkashvand A, Biparva P, Esfandiari M. Synthesis ratios of Mg-Al and Zn-Al layered double hydroxides efficiency and selectivity in nitrate removal from solution. Glob J Environ Sci Manag. 2019;5(4):485-500. doi: 10.22034/gjesm.2019.04.08.
45. Abdel-Hady EE, Mohamed HF, Hafez SH, Fahmy AM, Magdy A, Mohamed AS, et al. Textural properties and adsorption behavior of Zn-Mg-Al layered double hydroxide upon crystal violet dye removal as a low cost, effective, and recyclable

adsorbent. Sci Rep. 2023;13(1):6435. doi: 10.1038/s41598-023-33142-x.
46. Ivánová D, Albert P, Kavuličová J. Nitrate removal from model aqueous solutions and real water by calcined Mg/Al layered double hydroxides. Appl Clay Sci. 2018;152:65-72. doi: 10.1016/j.clay.2017.10.033.
47. Karthikeyan P, Meenakshi S. Synthesis and characterization of Zn–Al LDHs/activated carbon composite and its adsorption properties for phosphate and nitrate ions in aqueous medium. J Mol Liq. 2019;296:111766. doi: 10.1016/j.molliq.2019.111766.
48. Alagha O, Manzar MS, Zubair M, Anil I, Mu'azu ND, Qureshi A. Comparative adsorptive removal of phosphate and nitrate from wastewater using biochar-MgAl LDH nanocomposites: coexisting anions effect and mechanistic studies. Nanomaterials (Basel). 2020;10(2):336. doi: 10.3390/nano10020336.
49. Islam M, Patel R. Synthesis and physicochemical characterization of Zn/Al chloride layered double hydroxide and evaluation of its nitrate removal efficiency. Desalination. 2010;256(1-3):120-8. doi: 10.1016/j.desal.2010.02.003.
50. Shahbeig H, Bagheri N, Ghorbanian SA, Hallajisani A, Poorkarimi S. A new adsorption isotherm model of aqueous solutions on granular activated carbon. World Journal of Modelling and Simulation. 2013;9(4):243-54.